



HAL
open science

Capability Assessment of Five Different RANS-Based Turbulence Models to Simulate the Various Regions of Slot Turbulent Impingement Jet Flow

Mahmoud Charmiyan, Ahmed-Reza Azimian, Ebrahim Shirani, Fethi Aloui

► **To cite this version:**

Mahmoud Charmiyan, Ahmed-Reza Azimian, Ebrahim Shirani, Fethi Aloui. Capability Assessment of Five Different RANS-Based Turbulence Models to Simulate the Various Regions of Slot Turbulent Impingement Jet Flow. ASME 2017 Fluids Engineering Division Summer Meeting, Jul 2017, Waikoloa, United States. 10.1115/FEDSM2017-69203 . hal-03436532

HAL Id: hal-03436532

<https://uphf.hal.science/hal-03436532>

Submitted on 8 Jul 2022

HAL is a multi-disciplinary open access archive for the deposit and dissemination of scientific research documents, whether they are published or not. The documents may come from teaching and research institutions in France or abroad, or from public or private research centers.

L'archive ouverte pluridisciplinaire **HAL**, est destinée au dépôt et à la diffusion de documents scientifiques de niveau recherche, publiés ou non, émanant des établissements d'enseignement et de recherche français ou étrangers, des laboratoires publics ou privés.



Distributed under a Creative Commons Attribution 4.0 International License

CAPABILITY ASSESSMENT OF FIVE DIFFERENT RANS-BASED TURBULENCE MODELS TO SIMULATE THE VARIOUS REGIONS OF SLOT TURBULENT IMPINGEMENT JET FLOW

Mahmoud CHARMİYAN

m.charmiyan@gmail.com

Isfahan University of Technology, Department of
Mechanical Engineering, Isfahan, 8415683111,
Iran

Ebrahim SHIRANI

eshirani@gmail.com

Foolad Institute of Technology,
Department of Mechanical Engineering,
Fooladshahr, Isfahan, 84916 63763
Iran

Ahmed-Reza AZIMIYAN

azimian@cc.iut.ac.ir

Islamic Azad University, Khomeinishahr Branch,
Department of Mechanical Engineering,
Khomeinishahr, Iran

*** Fethi ALOUI**

** Corresponding author:*

fethi.aloui@univ-valenciennes.fr

LAMIH UMR CNRS 8201, University of
Valenciennes (UVHC), Department of Mechanical
Engineering, Campus Mont Houy, F-59313
Valenciennes Cedex 9 - France

ABSTRACT

In this paper, impingement of a turbulent rectangular flow to a fixed wall is investigated. The jet flows from bottom-to-top and the output jet Reynolds is 16000. The nozzle-to-plate distance is equal to 10 ($H/e=10$). Five turbulence models, including $k-\varepsilon$, RNG $k-\varepsilon$, $k-\omega$ SST, RSM and v^2f model have been used for two-dimensional numerical simulation of the turbulent flow. Because of the complexities of the impingement flow, such as curved streamlines, flow separation, normal strains and sudden deceleration in different areas, different turbulence models are proposed to simulate different regions of the flow. To investigate the capability of these turbulence models in simulating different regions of the impinging jet, the mean flow velocity field and turbulent kinetic energy are extracted and compared with the experimental data of a two-dimensional particle image velocimetry (PIV). The calculated error of these five turbulence models was presented for the various flow regions, while it has not been clearly investigated earlier. Results indicate the highest conformity of the v^2f model with the experimental data at the jet centerline. However, this

model does not predict well the flow at the shear layer and wall-jet areas. RSM Gibson and Lander model has the highest conformity with the experimental data in these regions.

Key words: Turbulent jet, Impinging jet, RANS-based turbulence models, Particle image velocimetry (PIV)

1. INTRODUCTION

Impinging of a jet flow to a wall is an effective and efficient way for the heat and mass transfer in the industrial applications. A high speed jet flow impinges a plate directly and increases the heat and mass transfer to a large extent. Many applications have been mentioned for this phenomenon in the literature. For example it is possible to mention metal industry, cooling of electronic components, defogging by heating optical surfaces, cooling turbine components and cooling sensitive parts in machining [1-3]. In this study, the impinging jet flow is divided into four regions. They are potential core, developing, impact and wall-jet regions (see Fig. 1). The characteristics of the mentioned regions are comprehensively described by Zuckerman and Lior

[4]. If the distance between the nozzle and plate is high, the jet behaves like a free submerged jet when it leaves the nozzle. In this case, the velocity variation in the jet edges creates a shear layer and consequently, momentum transfer happens. Therefore, more flow is drawn from the surrounding towards the jet and the mass flow increases. Hence, the energy dissipates and the velocity profiles become wider and its maximum reduces gradually.

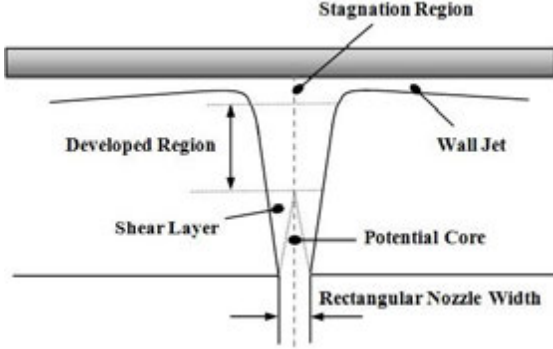


Fig. 1. Different region of a confined impingement jet flow

Due to the existence of different regimes as well as complications in the impingement of the turbulent jet to the walls, this problem has always used to test the validity and accuracy of the turbulence models. Since this phenomenon is widely used in simulating industrial processes, and the simulation of industrial processes by LES model is not cost effective, so investigating the strengths and weaknesses of the widely used RANS-based models is necessary. In the following paragraphs some more investigation found in the literature are presented.

Heyerichs and Pollard [5] simulated the turbulence jet impinging to the fixed wall using three different wall functions with five different damping functions. They concluded that the previously developed damping functions, which were dependent to distance from the wall (y^+), are sufficient to simulate the parallel and transient flows from the wall. However, they are not accurate for the impact area. Craft et al. [6] compared the numerical solution data of their model with experimental data of an impinging two dimensional jet to a wall. They observed that velocity at the centerline is estimated four times bigger than that of experimental data. Kubacki and Dick [7] simulated the impingement of a rectangular jet to the wall using $k-\omega$ model and three different hybrid models of $k-\omega/LES$. They investigated the shear stress of the wall and the heat transfer rate and reported a large difference between $k-\omega$ model and experimental data. Recently, Ortega-Casanova and Granados [6] studied the heat transfer between a circular air jet and a curved plate. They used $k-\epsilon$, $k-\omega$ SST and RSM model to simulate flow at different Reynolds numbers (between 7000 and 19000). They also examined the influence of the distance ratio on Reynolds number by varying the distance between the nozzle and wall to find the desired Reynolds number and distance ratio for

optimum heat transfer. However the flow structure is not considered at all. Zuckerman and Lior [4], compared different investigation results conducted in the field of simulating impinging jet in their review article.

Although considerable research have been conducted in the field of simulating jet impingement using RANS models, the majority of them were conducted to heat transfer of the circular jets and short impingement distances (Nozzle to plate distance). While, in the most of studies, the working fluid is air, the novelty of this work is the use of a fine space resolution of 2d-PIV measurements in water instead of air, in order to well check the validity of the chosen RANS-based turbulent models. In addition, in the most of previous works, characteristics of flow such as mean velocity field and turbulent kinetic energy at different regions of the jet impinging flow have not been clearly investigated.

In this study, the impingement of a rectangular turbulent jet to a wall is investigated both experimentally and numerically using five turbulence models $k-\epsilon$, RNG $k-\epsilon$, $k-\omega$ SST, RSM and v^2f for Reynolds number of 16,000. The distance of nozzle from the impingement wall is 10 times the nozzle width. Particle image velocimetry (PIV) data of Koched et al. [8] are extracted to evaluate the numerical simulation results.

2. GOVERNING EQUATIONS

To simulate the impingement of a turbulent isothermal jet to a wall, the time averaged continuity and momentum equations are used. Equations (1) and (2) represent the dimensionless averaged time averaged continuity and momentum equations for an incompressible fluid.

$$\frac{\partial \bar{u}_i}{\partial x_i} = 0 \quad (1)$$

$$\frac{\partial \bar{u}_i}{\partial t} + \frac{\partial \bar{u}_i \bar{u}_j}{\partial x_j} = -\frac{\partial \bar{P}}{\partial x_i} + \frac{1}{Re} \frac{\partial}{\partial x_j} \frac{\partial \bar{u}_i}{\partial x_j} - \frac{\partial \bar{\tau}_{ij}}{\partial x_j} \quad (2)$$

where \bar{u}_i and \bar{P} are the time average values of velocity and pressure, respectively, and $\bar{\tau}_{ij}$ is the Reynolds stress tensor. These equations are in dimensionless form using the output jet velocity and nozzle width. Reynolds stress tensor is given by equation (3).

$$\bar{\tau}_{ij} = \overline{u'_i u'_j} - \bar{u}_i \bar{u}_j \quad (3)$$

Many models have been proposed for modeling Reynolds stress term. In this study, five RANS-based turbulence models are used, which are illustrated with a brief explanation in the following sections.

2-1 k-ε standard model

The first two-equation model used in this study is k - ε standard model. This is the most widely used and economical model among the different turbulence models. The k - ε standard model is a semi-empirical model, solving the transfer equations for the turbulent kinetic energy k and its dissipation rate ε , respectively.

$$\frac{Dk}{Dt} = \frac{\partial}{\partial x_i} \left[\left(\mu + \frac{\mu_t}{\sigma_k} \right) \frac{\partial k}{\partial x_i} \right] + P^k - \varepsilon \quad (4)$$

$$\rho \frac{D\varepsilon}{Dt} = \frac{\partial}{\partial x_i} \left[\left(\mu + \frac{\mu_t}{\sigma_\varepsilon} \right) \frac{\partial \varepsilon}{\partial x_i} \right] + C_{1\varepsilon} \frac{\varepsilon}{k} P^k - C_{2\varepsilon} \frac{\varepsilon^2}{k} \quad (5)$$

where σ_k and σ_ε are kinetic turbulent Prandtl number and dissipation turbulent Prandtl number and are equal to 1 and 1.3, respectively. The model constants are $C_{1\varepsilon}=0.09$, $C_{1k}=1.44$ and $C_{2\varepsilon}=1.92$. Also, ρ is the fluid density and P^k is the production rate of turbulent kinetic energy. It is defined as follows.

$$P^k = -\rho \overline{u_i' u_j'} \frac{\partial u_j}{\partial x_i} = 2\mu_t S_{ij} S_{ij} \quad (6)$$

where S_{ij} is strain rate tensor and μ_t is the dynamic turbulent viscosity.

$$S_{ij} = \frac{1}{2} \left(\frac{\partial u_i}{\partial x_j} + \frac{\partial u_j}{\partial x_i} \right) \quad (7)$$

$$\mu_t = \rho C_\mu \frac{k^2}{\varepsilon} \quad (8)$$

2-2 RNG k-ε model

The RNG k - ε model includes a modification to the transport equation for ε stemming from renormalization group theory. The formulation of RNG k - ε model is consisted of the transfer equations for the turbulent kinetic energy k and dissipation rate ε , similar to k - ε model formulation (equations (4) and (5)), substituting $C_{2\varepsilon}$ with $C_{2\varepsilon}^*$ illustrated in equation (9).

$$C_{2\varepsilon}^* = C_{2\varepsilon} + \frac{C_\mu \eta^3 (1 - \eta / \eta_0)}{1 + \beta \eta^3} \quad (9)$$

where $\eta = Sk/\varepsilon$ and the turbulent viscosity being calculated in the same manner as with the standard k - ε model (equation (8)). The coefficients in equations (4), (5) and (9) are $\sigma_k=0.719$, $\sigma_\varepsilon=0.719$, $C_\mu=0.085$, $C_{1\varepsilon}=1.42$, $C_{2\varepsilon}=1.68$, $\beta=0.012$ and $\eta_0=4.38$.

2-3 k-ω SST model

The standard k - ω SST was first introduced by Menter [9] in 1994 and then, some of its coefficients were developed by Menter et al. [10] in 2003. In this study, the modified SST model is used as follows.

$$\rho \frac{Dk}{Dt} = \frac{\partial}{\partial x_i} \left[\left(\mu + \sigma_k \mu_t \right) \frac{\partial k}{\partial x_i} \right] + P^k - \rho \beta^* k \omega \quad (10)$$

$$\rho \frac{D\omega}{Dt} = \frac{\partial}{\partial x_i} \left[\left(\mu + \sigma_\omega \mu_t \right) \frac{\partial \omega}{\partial x_i} \right] + \alpha \rho S^2 - \beta \rho \omega^2 + 2(1 - F_1) \rho \sigma_{\omega 2} \frac{1}{\omega} \frac{\partial k}{\partial x_i} \frac{\partial \omega}{\partial x_i} \quad (11)$$

where F_1 is the blending function and is defined as follows.

$$F_1 = \tanh \left\{ \left[\min \left[\max \left(\frac{\sqrt{k}}{\beta^* \omega y}, \frac{500\nu}{y^2 \omega} \right), \frac{4\rho \sigma_{\omega 2} k}{CD_{k\omega} y^2} \right] \right]^4 \right\} \quad (12)$$

and

$$CD_{k\omega} = \max \left(2\rho \sigma_{\omega 2} \frac{1}{\omega} \frac{\partial k}{\partial x_i} \frac{\partial \omega}{\partial x_i}, 10^{-10} \right) \text{ and } y \text{ is the}$$

distance from the nearest wall. The value of F_1 in the far from the surfaces and inside the boundary layer is equal to zero (k - ε model) and equal to one (k - ω model), respectively. In this model, the turbulent viscosity is illustrated by equation (13).

$$\nu_t = \frac{a_1 k}{\max(a_1 \omega, S F_2)} \quad (13)$$

In which, S is the invariant of strain rate and F_2 is the second blending function illustrated by equation (14).

$$F_2 = \tanh \left[\left[\max \left(\frac{2\sqrt{k}}{\beta^* \omega y}, \frac{500\nu}{y^2 \omega} \right) \right]^2 \right] \quad (14)$$

It should be noted that in SST model, a restrictive term is used for the production term in order to not overestimate the turbulence in stagnation regions (equation 15).

$$P_k = \mu_t \frac{\partial U_i}{\partial x_j} \left(\frac{\partial U_i}{\partial x_j} + \frac{\partial U_j}{\partial x_i} \right) \quad (15)$$

$$\rightarrow P_k = \min(P_k, 10 \cdot \beta^* \rho k \omega)$$

The constants used in equations (10) and (11) are $\alpha_1=5/9$, $\beta_1=3/40$, $\beta_2=0.0828$, $\sigma_{\omega 1}=0.5$, $\sigma_{\omega 2}=0.856$, $\sigma_{k1}=0.85$, $\sigma_{k2}=1$ and $\beta^*=0.09$.

2-4 Reynolds stress transport models (RSM)

In RSM models, there are exact transport equations for Reynolds stress terms, $u_i u_j$ (equation (16)).

$$\begin{aligned} \frac{\partial}{\partial x_k} \left(U_k \overline{u_i u_j} \right) &= -\overline{u_i u_k} \frac{\partial U_j}{\partial x_k} - \overline{u_j u_k} \frac{\partial U_i}{\partial x_k} \\ &- \frac{\partial}{\partial x_k} \left(\overline{u_i u_j u_k} + \frac{1}{\rho} \delta_{jk} \overline{u_j p} - \nu \frac{\partial \overline{u_i u_j}}{\partial x_k} \right) \\ &+ \frac{p}{\rho} \left(\frac{\partial u_i}{\partial x_j} + \frac{\partial u_j}{\partial x_i} \right) - 2\nu \frac{\partial u_i}{\partial x_k} \frac{\partial u_j}{\partial x_k} \end{aligned} \quad (16)$$

A review of second-moment computations for engineering flows has been provided by Leschziner [11] and Launder [12]. Results of these computations demonstrate the superiority of RSMs over eddy-viscosity models for curved flows, swirling flows, buoyant flows and recirculating flows.

In the present study, the model proposed by Gibson and Launder [13] has been chosen mainly because it takes into account the influence of a wall on the pressure field. The mentioned characteristic causes some advantage to simulate the decelerating and stagnation regions with high fluctuations in the pressure field.

2-5 v^2f model

This model was first introduced in 1991 by Durbin [14]. In this model, two equations are added to the $k-\varepsilon$ model and therefore, a 4-equation model is achieved. One equation for turbulent stresses perpendicular to the flow stream lines (v^2) and another as a function f to estimate the effects of the wall on the changes of v^2 . In this study, a modified model by Davidson et al. [15] is used. Equations 17 and 18 are used to calculate v^2 and f .

$$\frac{Dv^2}{Dt} = kf_{wall} - v^2 \frac{\varepsilon}{k} + \frac{\partial}{\partial x_j} \left[(v+v') \frac{\partial v^2}{\partial x_j} \right] \quad (17)$$

$$f_{wall} - I_{scale}^2 \frac{\partial}{\partial x_j} \frac{\partial f}{\partial x_j} = \frac{(C_1 - 1) \left(\frac{2}{3} - \frac{v^2}{k} \right)}{T_{scale}} + \frac{C_2 2v' S_{ij} S_{ij}}{k} \quad (18)$$

where L_{scale} and T_{scale} shows length and time scales respectively, and $v' = C_\mu v^2 T_{scale}$. The models constants are $C_1=1.4$, $C_2=0.3$ and $C_\mu=1.9$.

3. NUMERICAL SCHEME AND METHOD OF SOLUTION

3.1 Numerical method

The numerical platform is an open source CFD code based on the field operation and manipulation C++ class library for continuum mechanics (OpenFOAM 2.3.0) and is used to simulate the flow and represent the mean and instantaneous flow field

characteristics. The program uses collocated grid arrangement and the pressure-velocity coupling is handled with SIMPLE¹ [16]. The convective terms in the momentum equations are discretized using the second-order, bounded van Leer scheme [17]. The convective terms in the equations for turbulent quantities are discretized with hybrid upwind/central differencing.

3.2 Computational domain

Fig. 2 represents the schematic of two dimensional computational domain and boundary conditions of the problem. As shown in Fig. 2, the nozzle width (e) is equal to 20 mm and the distance of nozzle from the plate (H) is $10e$ based on the Maurel and Sollicie [18] study. They stated that a maximum turbulence intensity of the vertical component of the velocity field is occurred at the distance $H/e=10$. Therefore, in this distance one can be sure that the jet flow is fully turbulent when it hits the plane.

The channel length (L_{ch}) is $15e$ and the total domain length (L_x) is equal to $85e$. There are two outlet boundary conditions in both sides of the impingement plate. The length of these two outlet domains (L_{out}) are $5e$. The aforementioned sizes of the computational domain are chosen from experimental setup data [8].

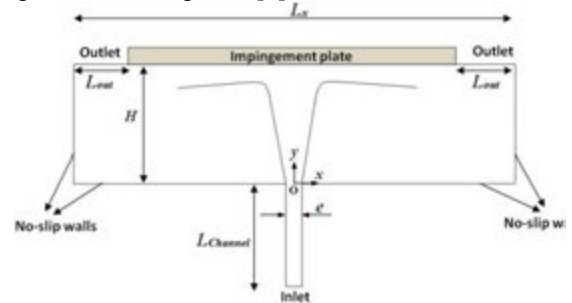


Fig. 2. Schematic of computational domain and boundary conditions

3.3 Boundary conditions

All boundary conditions are shown in Fig. 2. The inlet bulk velocity is $u_{in}=0.75$ m/s. A parametric study of the inlet velocity is performed to approximate the inlet profile with conformity the experimental data used. As shown in Fig. 3, comparison to the experimental inlet values, it is observed that $L_{ch}/e=15$ is the value that better fits our requisites, $Re=16000$. Turbulent kinetic energy in the nozzle exit is equal to that obtained from the PIV data [8].

¹ semi-implicit method for pressure-linked equations

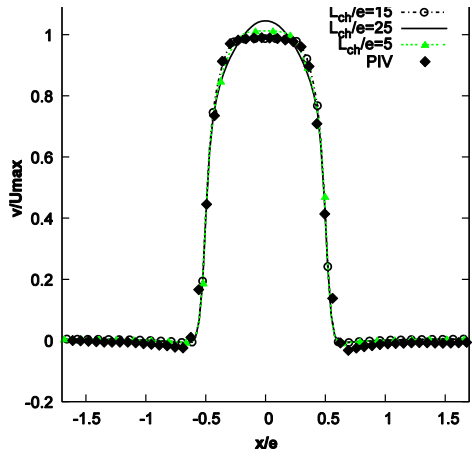


Fig. 3. Parametric study of the inlet boundary condition at the nozzles exit compared against PIV results

The output boundary condition is considered as constant pressure and its value is equal to the atmospheric pressure.

No slip boundary condition is considered as at the channel wall, chamber wall and impingement plate. A wall function has been used for all simulation and the first grid point near the wall has been ensured to fall in the logarithmic region, i.e., $30 < Y^+ < 100$ where $Y^+ = yu_t/\nu$, u_t being the friction velocity.

The rate of dissipation (ε) and the rate of specific dissipation (ω) are taken equal to $\varepsilon = C_\mu^{3/4} k^{3/2} / 0.07e$ and $\omega = k^{1/2} / 0.07C_\mu^{1/4}$ at the inlet for $k-\varepsilon$ model (also RNG $k-\varepsilon$) and $k-\omega$ SST. In Reynolds stress model turbulence is assumed to be isotropic at the inlet and all normal components of Reynolds stresses are given the value $2k/3$, whereas all shear Reynolds stresses are set to zero. Similarly, v^2 and f are equal to $2k/3$ with zero gradient at the inlet for v^2f model. At the walls v^2 and f are assumed to be 0 and $(20v^2v^2)/(\varepsilon y^4)$, respectively.

3-4 Grid study

To ensure the independency of results from computational grid size, four different grids are studied. These grids are named as case 0 to case 3 and contain 19,280, 34,280, 80,480 and 101,980 cells, respectively. In all cases, the mesh sizes are fine near the impingement plate and near the jet center.

Fig. 4 indicates the longitudinal components of the mean flow velocity field near the impingement plate ($y/H=0.9$) and also on the parallel line with the impingement plate for $k-\varepsilon$ and $k-\omega$ SST models. As seen in these figures, all four grids predict very close results for the mean velocity components, while according to the turbulent flow characteristics (such as turbulent kinetic energy) this condition is not acceptable. From results obtained for TKE in Figs. 4 a-d, case 2 is used in this study.

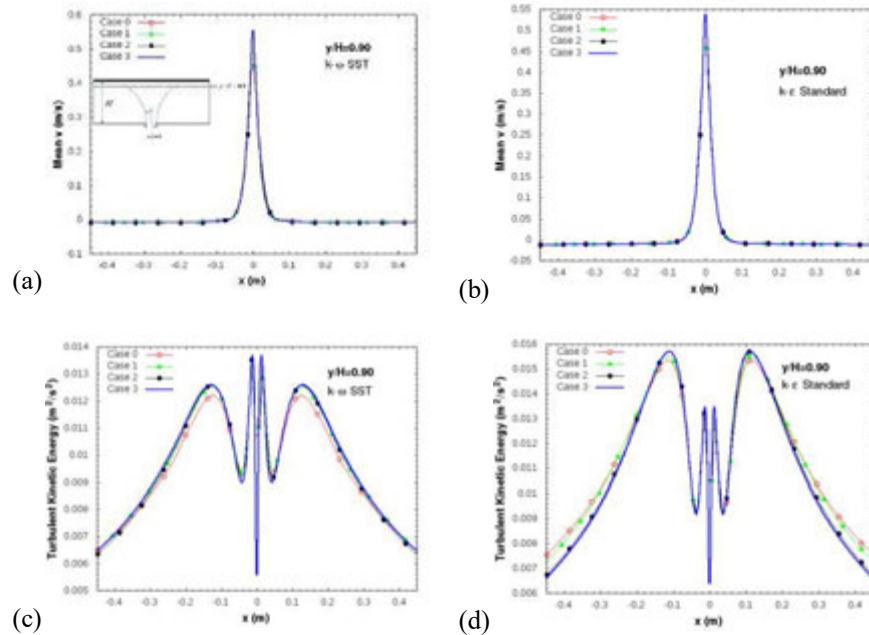


Fig. 4. Grid independency test using mean longitudinal velocity component and turbulent kinetic energy

4. RESULTS

In this section, results obtained for five turbulence models, $k-\varepsilon$, RNG $k-\varepsilon$, $k-\omega$ SST, RSM and v^2f , are presented for impingement of the water

jet to a wall with $Re=16000$ in comparison with the experimental data at different impinging jet regions.

Fig. 5 shows the longitudinal velocity component profile obtained from aforementioned RANS-based turbulence models at jet centerline in comparison

with $k-\omega$ model (Kubacki and Dick [7]) and PIV data. It is seen that the $k-\omega$ model, has more error compared to the other models and estimates the potential core length about $0.79H$ (where the mean velocity is almost constant). As it can be seen in Fig. 5, the potential core lengths are $0.72H$, $0.78H$, $0.72H$, $0.49H$ and $0.31H$ for $k-\varepsilon$, RNG $k-\varepsilon$, $k-\omega$ SST, RSM and v^2f models, respectively. The potential core length obtained from PIV data is about $0.3H$.

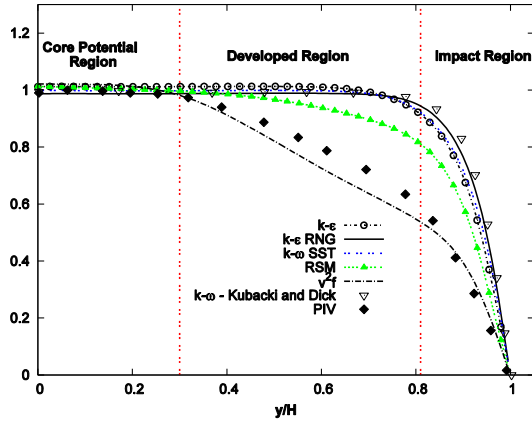


Fig. 5. Comparison of dimensionless wall-normal velocity obtained by five turbulence models at jet center line with $k-\omega$ [7] and PIV data

In the next sections, flow simulation is done using different turbulence models at three main impinging jet regions.

4-1 Potential core region

The main characteristic of this region is uniformity of the velocity at jet centerline. When the nozzle-to-plate distance is 10 times the nozzle width, the potential core region continues up to $y/e=3$ (Fig. 5). As it is seen from Fig. 6, by moving away from the nozzle, the jet grows and the impact region on the surrounding fluid extends to $x/e=1$ (Fig. 6-c). However, the maximum velocity on the jet centerline is almost constant. In this region, the best agreement between the numerical results and experimental data is observed. By moving away from the nozzle, only the RNG $k-\varepsilon$ model indicates the value of the longitudinal mean velocity component slightly less than the experimental one. In the entrainment region (formed on either side of the jet centerline and the surrounding fluid is drawn towards the jet), RSM and v^2f models show a lower values for the mean longitudinal velocity component compared to the experimental data (Figs. 6b-c).

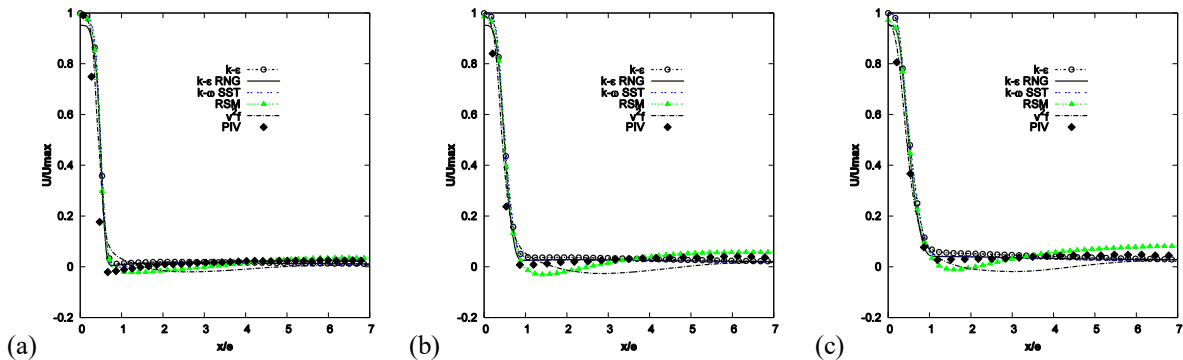


Fig. 6. Transverse profile of non-dimensional longitudinal mean velocity component in potential core region. (a) $y/e=1$, (b) $y/e=2$ and (c) $y/e=3$.

As shown in Fig. 7, $k-\varepsilon$, RNG $k-\varepsilon$ and $k-\omega$ SST models predict the dimensionless turbulent kinetic energy in the potential core close to zero, which is much lower than that of experimental data. While RSM and v^2f predict higher values (about 0.005 for $y/e=3$). However, the value of the dimensionless turbulent kinetic energy from the experimental data is higher and is equal to 0.004, 0.008 and 0.0014 for

$y/e=1$, $y/e=2$ and $y/e=3$, respectively. Moving away from the jet centerline to the either sides, the turbulent kinetic energy is increased due to the impingement of the jet to the surrounding fluid and reaches to its highest value. In the potential core, all models but RNG $k-\varepsilon$, over predict the maximum value of turbulent kinetic energy.

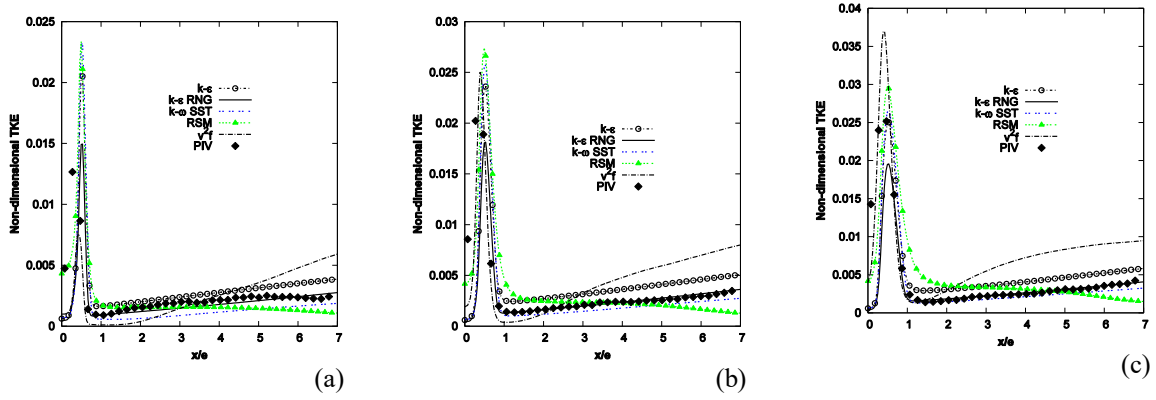


Fig. 7. Non-dimensional Turbulent Kinetic Energy (TKE) across horizontal lines in potential core region. (a) $y/e=1$, (b) $y/e=2$ and (c) $y/e=3$.

4-2 Developing region

Fig. 8 represents the longitudinal mean velocity profiles in the developing region, calculated by different turbulence models in comparison with experimental data for different sections. By approaching the stagnation region, the difference between the simulated velocity profiles at the centerline with the experimental data gradually increases. The longitudinal velocity component calculated by $k-\varepsilon$ and $k-\omega$ SST models in the developing region (up to $y/e=7$) is almost constant and is equal to the nozzle exit velocity. It then decreases slightly up to $y/e=8$. These two models overestimate the value of the longitudinal velocity component by about 70% at the centerline. Accuracy of the mean longitudinal velocity predicted by RNG $k-\varepsilon$ model is slightly better than the other models.

However, among the mentioned models, the maximum under prediction of the velocity in the shear layer region is obtained by $k-\varepsilon$ model. The RSM model predicts the average longitudinal velocity much better than the other three models. By approaching to the decelerating region, the pressure-strain rate increases compared to the other terms in the momentum equation. So, this model is able to predict the velocity in this region better than previous models. However, the constant coefficients in the presented models are not accurate for strain-pressure term in impinging flows. Therefore, the model is faced with restrictions to simulate the flow in this area. The vertical velocity component results obtained by v^2f model have the best agreement with PIV data. However, the accuracy decreases by approaching the impingement wall (Figs. 8 a-e).

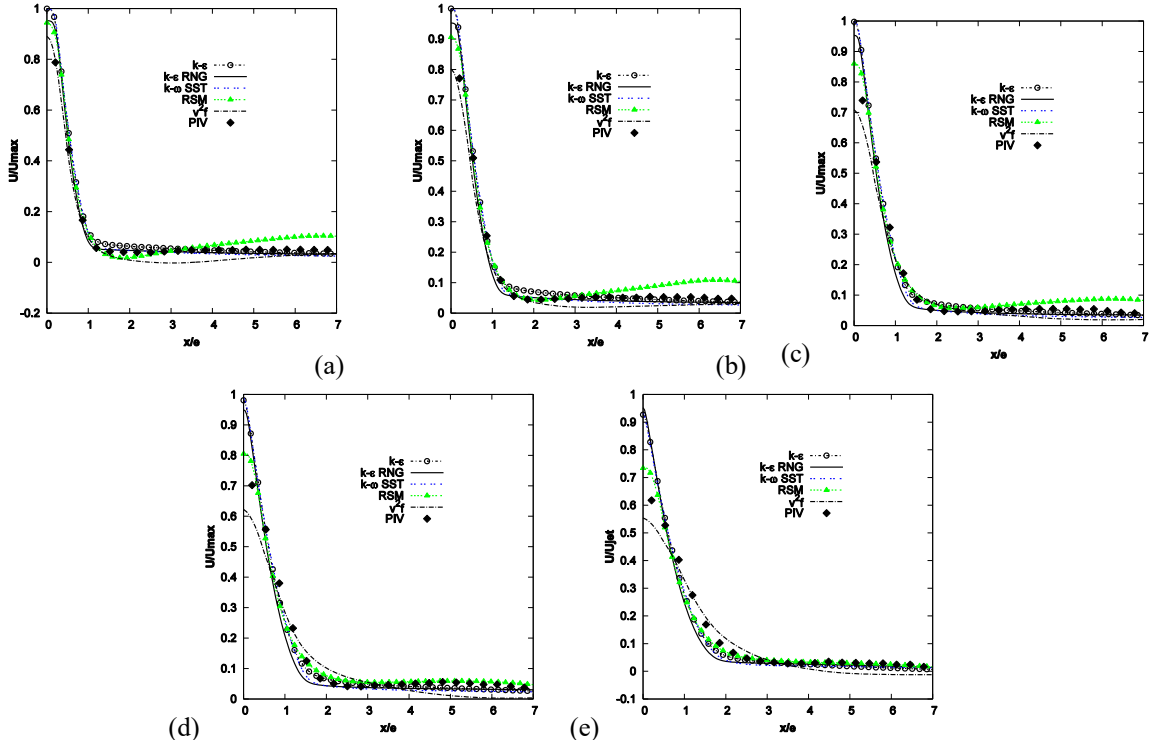


Fig. 8. Non-dimensional wall-normal velocity across horizontal lines in developing region. (a) $y/e=4$, (b) $y/e=5$, (c) $y/e=6$, (d) $y/e=7$ and (e) $y/e=8$.

Figures. 9a to 9e represent the non-dimensional TKE achieved from various turbulence models and also from experimental data. Unlike the potential core region in which most of the models over-estimate the turbulent kinetic energy compared to the experimental data, in this region the maximum energy (in the shear layer) is under-estimated by most of the models. Only the v^2f model overestimates the value of the maximum energy. As it is seen from Fig. 9, similar to the potential core

region, three models of $k-\epsilon$, RNG $k-\epsilon$ and $k-\omega$ SST, estimate the TKE value in the jet centerline near zero. However, by moving away from the jet centerline and shear layer, TKE value is over predicted. Among the five models, RSM and v^2f models estimate the kinetic energy in the shear layer region more accurately. However, The RSM model estimates the value of TKE less than the experimental data and v^2f model estimates the value higher than experimental data.

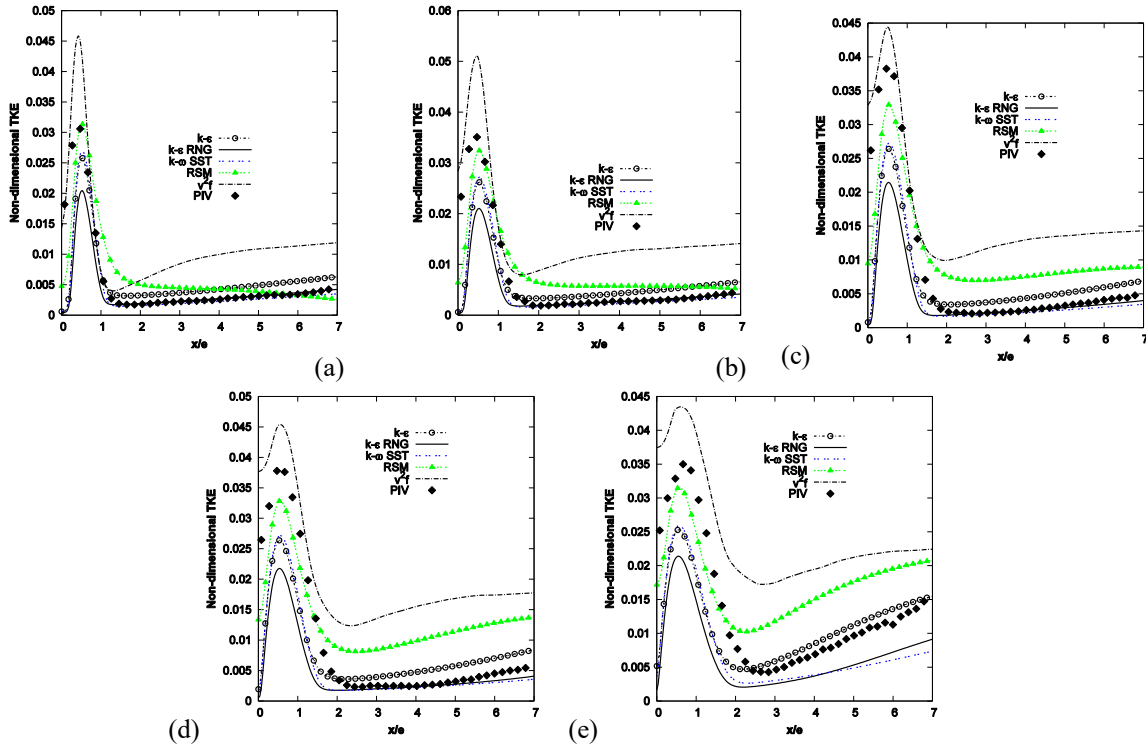


Fig. 9. Non-dimensional Turbulent Kinetic Energy (TKE) across horizontal lines in developing region. (a) $y/e=4$, (b) $y/e=5$, (c) $y/e=6$, (d) $y/e=7$ and (e) $y/e=8$.

4-3 Impact region

Figs. 10-a to 10-c represent the velocity profiles in the impact region. As it can be seen, the RSM and v^2f models provide a good estimation of the mean longitudinal velocity near the jet centerline.

RSM not only allows transport and development of the individual Reynolds stresses. They also have the advantage that terms accounting for anisotropic effects are introduced automatically into the stress

transport equations. These non-isotropic characteristics of the turbulence play very important role in the flows with streamline curvature, swirl or strong recirculation. However, despite the reasonable estimation of RSM model, it does not have good accuracy in calculating the velocity field in the shear layer. In fact, all of the studied models under-estimate the value of velocity in the shear layer region ($x/e > 1$).

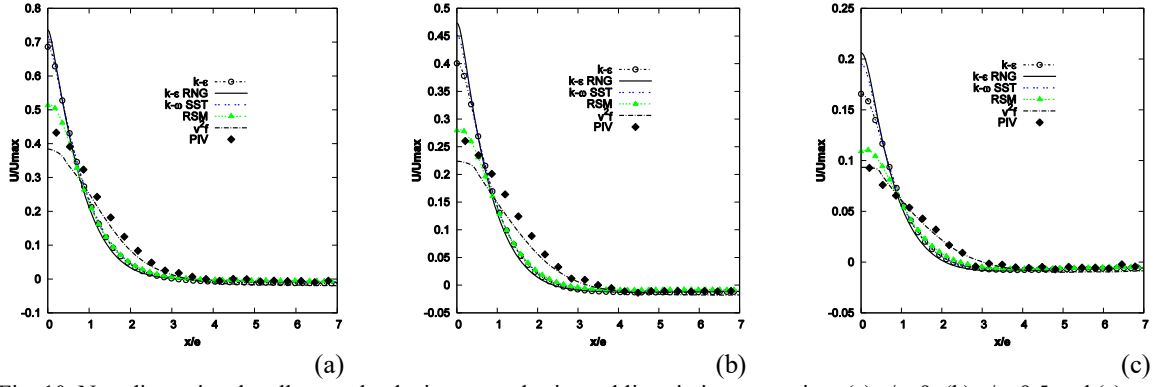


Fig. 10. Non-dimensional wall normal velocity across horizontal lines in impact region. (a) $y/e=9$, (b) $y/e=9.5$ and (c) $y/e=9.8$.

The largest difference between the numerical and experimental results is observed for turbulent kinetic energy in the impact region. The dimensionless turbulent kinetic energy of the jet is increased in the centerline of the jet in this region and reaches to 0.035 in $y/e=9.5$ (Fig. 11-b). The flow tends to the either sides and a boundary layer near the wall-jet

region forms. Therefore, the value of TKE is not decreased to zero by moving away from the jet centerline. As it is seen from Figs. 11-a to 11-c, RNG $k-\epsilon$ and $k-\omega$ SST models estimate the value of TKE in the jet centerline very poor. However agreement between the models results and experimental ones in the wall-jet region is good.

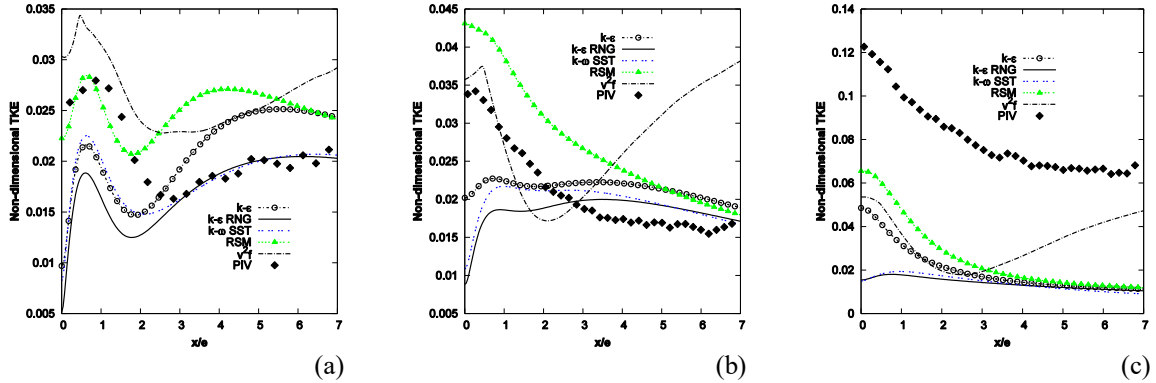


Fig. 11. Non-dimensional Turbulent Kinetic Energy (TKE) across horizontal lines in impact region. (a) $y/e=9$, (b) $y/e=9.5$ and (c) $y/e=9.8$.

Estimation of TKE by $k-\epsilon$ model is higher than the two previously mentioned models and still a large difference between these results and the experimental data is observed. TKE values obtained by RSM and v^2f models are slightly over-estimated on the jet centerline at $y/e=9$ and 9.5. However TKE at $y/e=9.8$ obtained from PIV data is much higher than simulated using different turbulence models.

The maximum errors percentage of velocity stated by equation (19) of the various turbulence models for different regions are presented in table 1.

$$Error = \left| \frac{V_{Simulation} - V_{Experiment}}{V_{Experiment}} \right| \times 100 \quad (19)$$

Table 1. Longitudinal velocity component maximum error (%) of different turbulence models in different impingement jet regions at jet center line

Models	$k-\epsilon$	$k-\epsilon$ RNG	$k-\omega$ SST	RSM	v^2f
Potential core region	2%	7%	4%	2.5%	2%
Developing region	48%	50%	46%	16%	12%
Impact region	75%	80%	75%	28%	25%

5- CONCLUSIONS

In this paper, the turbulent slot impinging flow is simulated using five RANS-based turbulence models at $Re=16000$ and the results are compared with the experimental data. In order to have fully turbulent flow, the nozzle-to-wall distance was considered sufficiently large ($H/e=10$). In order to investigate the impingement of a jet to a wall numerically and experimentally, the mean velocity field and the turbulent kinetic energy are considered. The numerical simulations were conducted by five most used models in the industrial processes, including $k-\varepsilon$, RNG $k-\varepsilon$, $k-\omega$ SST, RSM and v^2f and the obtained results were compared with each other. The main novelty of this work is the use of a fine space resolution of 2D-PIV measurements (resolved in time) in a turbulent impinging water jet configuration (low velocity compared to that of air using similarity, so good accuracy) in order to well check the validity of the tested RANS turbulent models in different flow regions.

- All checked models simulate correctly the mean velocity field with rather great accuracy in the potential core region so that the maximum error is about 7% belonging to the RNG $k-\varepsilon$ model. However the error estimated for turbulent kinetic energy in this region is large and reaches its highest value for the shear layer region.
- The $k-\varepsilon$, RNG $k-\varepsilon$ and $k-\omega$ SST models estimate the potential core length about 2.5 times more than the experimental values while the RSM and v^2f models estimate this length 1.6 and 1.03 times bigger, respectively.
- Comparison of the average velocity field obtained from the numerical and experimental results indicates that the estimated value by two-equation turbulence models (RNG $k-\varepsilon$, $k-\omega$ SST and $k-\varepsilon$) involved with errors up to 100%, which is maximum in the decelerating regions.
- Precision of calculated velocity profiles at the jet centerline is very high in the RSM model. However, this model shows a high error (71%) in predicting the kinetic energy in the developing region at $y/e=6$. In this region, the results of v^2f present the highest consistency with the experimental data, which indicates the validity of considering the pressure perturbation and wall effect in calculating v^2 and f functions, respectively.
- The maximum error in calculating TKE was observed in the impact region, in which the sudden change in the direction of the velocity vector in addition to non-isotropic nature of the flow was resulted in an inaccurate modeling of the turbulence viscosity (ν_t) and the turbulent kinetic energy. The RSM and v^2f results show the highest agreement with the experimental data. It seems that by improving the constant in these models, better agreement is achieved.

- Although the v^2f model is successfully estimates the time averaged velocity field in three potential core, developing and impact regions, especially on jet centerline, however, it showed the highest error in estimating the turbulent kinetic energy in the wall-jet region. This reflects the failure of this models to predict the vertex deformation in the impact area and formation of the boundary layer.

ACKNOWLEDGMENTS

This work was supported by the laboratory LAMIH CNRS UMR 8201 (University of Valenciennes, France), the Department of Mechanical Engineering (Isfahan University of Technology, Iran) and the Department of Mechanical Engineering (Islamic Azad University, Khomeinishahr Branch, Iran). These supports are gratefully acknowledged.

REFERENCES

- [1] J. Ferrari, N. Lior and J. Slycke, An evaluation of gas quenching of steel rings by multiple-jet impingement, *Journal of materials processing technology*, 136, 1 (2003), 190-201.
- [2] J.-C. Han, Recent studies in turbine blade cooling, *International Journal of Rotating Machinery*, 10, 6 (2004), 443-457.
- [3] O. Lyons, D. Murray and A. Torrance, Air jet cooling of brake discs, *Proceedings of the Institution of Mechanical Engineers, Part C: Journal of Mechanical Engineering Science*, 222, 6 (2008), 995-1004.
- [4] N. Zuckerman and N. Lior, Jet impingement heat transfer: Physics, correlations, and numerical modeling, *Advances in heat transfer*, 39, 06 (2006), 565-631.
- [5] K. Heyerichs and A. Pollard, Heat transfer in separated and impinging turbulent flows, *International Journal of Heat and Mass Transfer*, 39, 12 (1996), 2385-2400.
- [6] T. Craft, L. Graham and B. E. Launder, Impinging jet studies for turbulence model assessment-II. An examination of the performance of four turbulence models, *International Journal of Heat and Mass Transfer*, 36, 10 (1993), 2685-2697.
- [7] S. Kubacki and E. Dick, Simulation of plane impinging jets with $k-\omega$ based hybrid RANS/LES models, *International Journal of Heat and Fluid Flow*, 31, 5 (2010), 862-878.
- [8] A. Koched, M. Pavageau and F. Aloui, Vortex structure in the wall region of an impinging plane jet, *Journal of Applied Fluid Mechanics*, 4, 2 -s 1 (2011), 61-69.
- [9] F. Menter, Zonal two equation $k-\omega$ turbulence models for aerodynamic flows., *AIAA paper*, (1993), 96-2906.

- [10] F. Menter, M. Kuntz and R. Langtry, Ten years of industrial experience with the SST turbulence model, *Turbulence, heat and mass transfer*,4, 1 (2003).
- [11] M. Leschziner, Modelling engineering flows with Reynolds stress turbulence closure, *Journal of Wind Engineering and Industrial Aerodynamics*,35 (1990), 21-47.
- [12] B. E. Launder, Second-moment closure: present... and future?, *International Journal of Heat and Fluid Flow*,10, 4 (1989), 282-300.
- [13] M. Gibson and B. Launder, Ground effects on pressure fluctuations in the atmospheric boundary layer, *Journal of Fluid Mechanics*,86, 03 (1978), 491-511.
- [14] P. A. Durbin, Near-wall turbulence closure modeling without “damping functions”, *Theoretical and Computational Fluid Dynamics*,3, 1 (1991), 1-13.
- [15] L. Davidson, P. V. Nielsen and A. Sveningsson, Modifications of the $\bar{U}2$ -Model for Computing the Flow in, Proceedings of the International Symposium on Turbulence,(2003).
S. Patankar *Numerical heat transfer and fluid flow*, CRC press1980).
- [17] B. Van Leer, Towards the ultimate conservative difference scheme. II. Monotonicity and conservation combined in a second-order scheme, *Journal of computational physics*,14, 4 (1974), 361-370.
- [18] S. Maurel and C. Sollicc, A turbulent plane jet impinging nearby and far from a flat plate, *Experiments in Fluids*,31, 6 (2001), 687-696.